NASA

Technical Memorandum 79565

# Determining Crustal Strain Rates with a Spaceborne Geodynamics Ranging System Data, 1, Baseline Analysis

Steven C. Cohen and Glenn R. Cook



JUNE 1978

National Aeronautics and Space Administration

**Goddard Space Flight Center**
Greenbelt, Maryland 20771

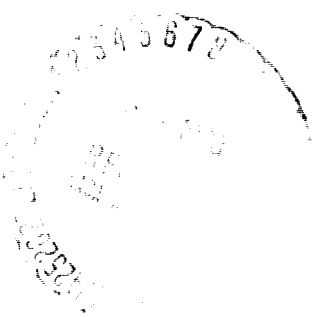

TM 79565

# DETERMINING CRUSTAL STRAIN RATES WITH A SPACEBORNE GEODYNAMICS RANGING SYSTEM DATA, 1, BASELINE ANALYSIS

Steven C. Cohen
Glenn R. Cook
Geodynamics Branch

June 1978

GODDARD SPACE FLIGHT CENTER

Greenbelt, Maryland

# DETERMINING CRUSTAL STRAIN RATES WITH A SPACEBORNE GEODYNAMICS RANGING SYSTEM DATA, 1, BASELINE ANALYSIS

Steven C. Cohen
Glenn R. Cook
Geodynamics Branch

## ABSTRACT

The Spaceborne Geodynamics Ranging System is a proposed satellite-borne laser ranging system which would be capable of making highly precise geodetic measurements over baselines ranging from a few tens of kilometers to several hundred kilometers. In this paper we analyze the precision with which crustal strain rates could be derived from measurements made with this system. Using simple site configurations, intersite distances of about 25-70 kilometers, and measurement programs ranging from a few years to fifteen years, we conclude that precisions of several parts in $10^9$ per year are achievable. Compared to the expected shear strain rates of about $7 \times 10^{-7}$ $yr^{-1}$, this produces very favorable signal-to-noise ratios. By using scaling laws, the results obtained here may also be used for other combinations of baseline distances, measurement times, and precisions in baseline determinations.

# DETERMINING CRUSTAL STRAIN RATES WITH A SPACEBORNE GEODYNAMICS RANGING SYSTEM DATA, 1, BASELINE ANALYSIS

## I. INTRODUCTION

The Spaceborne Geodynamics Ranging System (SGRS) is a proposed laser ranging system which would be carried on board a spacecraft and used for precision determination of the relative locations of groundpoints on which reflective targets have been mounted. It is, in a sense, the inverted version of the ground based laser tracking system that has been used for a number of years for high accuracy satellite tracking and precision geodesy. Since the SGRS system has the potential capability to measure changes in the relative horizontal and vertical locations of targets spaced from tens to hundreds of kilometers apart to precisions of a few centimeters, it is an attractive candidate for use in a number of fundamental and applied crustal geodynamics measurements. Among these measurements are relative motions of tectonic plates across the plate boundaries, crustal deformations prior to and after major earthquakes, land subsidence due to fluid extraction, and edifice building associated with volcanoes. In this paper we focus attention on one, perhaps primary, application for the SGRS system namely the determination of the rates of crustal straining and the measurement of the spatial extent of the strain field in regions of active strike-slip faulting. The San Andreas fault system in California serves as an excellent example of a location suitable for the measurement of crustal strain with a SGRS system.

Previous analyses of SGRS-type systems have focused either on the state of engineering development or the analysis of the accuracy expected in the measurement of the intersite vectors. These analyses serve as the departure point for

the present paper which concentrates on its utility as a geodetic tool. The paper is organized in the following manner. In section II we describe the SGRS concept, its current state of development, and the expected precision in the intersite distance measurements. We begin section III by reviewing the concepts of crustal strain and formulate mathematical procedures for deducing strain rates from the measured intersite distances. We then present numerical results showing the deduced precision in the SGRS determination of the rates and compare these precisions to the current estimates of the strain rates along the strike-slip fault systems in California. The fourth section summarizes our findings and current thoughts on the utility of the SGRS system.

## II. SYSTEM DESCRIPTION AND CAPABILITIES

A conceptual representation of a SGRS measurement is shown in Figure 1. An orbiting spacecraft is equipped with a laser tracking system which includes in addition to the laser, a precision acquisition and pointing system, return pulse detection electronics, and timing devices. The laser fires frequent short duration pulses at cube corner reflectors located in a grid in a ground target area. In a sequential manner pulses are sent to each of the reflective targets and the round trip travel times measured. These travel times are converted in the data analysis to ranges. With a suitably large number of measurements, a model of the earth's gravitational field, an a-priori trajectory estimate for the satellite and various system corrections, it is possible to determine the target locations and the intersite vectors between the various stations. Such computations have been described by Vonbun, et al (1977) and Gibbs and Haley (1978). In the version of SGRS currently under development only one target reflector is illuminated at a time. Further developments may make possible the simultaneous illumination

of two or more reflectors. Current specifications for a system under development and proposed for flying onboard the space shuttle are shown in Table I. The engineering status of the system is well advanced. The space qualified Nd:YAG laser transmitter has a 50 millijoule output at 0.53 $\mu$m and can be triggered at ten pulses per second. The electro-optical-mechanical pointing system has been designed and is under construction. The prototype cube corner reflective arrays are designed with a number of cube corner reflectors mounted on a hemispherical surface. The expected signal-to-noise ratio at the Shuttle is 20 db at 90° elevations and 7 db at 20° elevations. The precision in measuring the pulse time of flight is expected to correspond to a range precision of ten centimeters or better and, after data processing, the precision in the intersite vectors is estimated at better than two centimeters in both the vertical and horizontal components for baselines less than about 100 kilometers (Gibbs and Haley, 1978). This precision ignores some additional bias due to modelling errors in the gravity field. At the level of discussion in this paper, this additional bias does not effect the measurement of the rate of change of the intersite distances, which is the input parameter of interest. For baselines of several hundred kilometers the precision in the horizontal component is again expected to be a few centimeters, but the precision in the vertical components degrades to about 4 centimeters at 400 kilometers. (Kahn, private communication).

## III. STRAIN ANALYSIS

SGRS is essentially a surveying device which determines the location of various target sites. In the present context we wish to interpret changes in the locations in terms of the accumulations of crustal strain. It is the degree of strain accumulation, its spatial distribution and its rate of accumulation that are

important in studying a host of geophysical problems including the causes and prediction of earthquakes, the interactions of tectonic plates, and the formation of geologic structures. We will present our discussion of strain accumulation in two dimensions, the generalization to three dimensions can be made by inspection.

There are a number of different ways in which the data obtained from a SGRS measurement can be employed in strain analyses. One method involves working directly with the deduced target site coordinates determined during several different missions and using the definitions of the strain components discussed below. An alternative technique is to work not with the site locations themselves but rather with the baseline distances between sites. This is the approach we have chosen; there are a number of reasons for having done so. By working with baselines rather than site locations we avoid potential problems in defining a stable reference frame in which site coordinates can be expressed. All that is necessary to derive the strain rates are the changes in intersite distances from one survey to another and not the changes in the locations of each point. Since it is entirely possible that baselines changes can be deduced to a greater precision that site location changes this point may be significant. The analysis we perform is also very general in the sense that it requires only baseline distances and is independent of how such distances have been obtained. Thus data from SGRS, alternative space techniques, and ground surveys can all be processed in the same manner and the techniques we have used here are equally applicable for all such systems.

The potential penalty we pay for adopting this approach is that we do not use all the data that might be available from the measurements. These additional

pieces of data may permit deduction of strain rates to a greater precision than we indicate in the present paper. This point will be pursued more at a later date.

Consider as in Figure 2 an initially unstrained line of length $r_o$ from point $(x_1, y_1)$ to point $(x_2, y_2)$. After straining the line length is r and the coordinates of the two points are $(x_1 + u_1, y_1 + v_1)$ and $(x_2 + u_2, y_2 + v_2)$. The elongation of the line, $\epsilon$, is defined as

$$\epsilon = \frac{r - r_o}{r_o} = \frac{\sqrt{(x_2 + u_2 - x_1 - u_1)^2 + (y_2 + v_2 - y_1 - v_1)^2} - \sqrt{(x_1 - y_1)^2 + (y_2 - y_1)^2}}{\sqrt{(x_2 - x_1)^2 + (y_2 - y_1)^2}} \quad (1)$$

If we now assume that $u_2 - u_1$ and $v_2 - v_1$ are sufficiently small compared to $x_2 - x_1$ and $y_2 - y_1$ (this is the assumption of infinitesimal strain) it follows that

$$\epsilon = \frac{(x_2 - x_1)(u_2 - u_1) + (y_2 - y_1)(v_2 - v_1)}{(x_2 - x_1)^2 + (y_2 - y_1)^2} = \frac{r_o \cdot \Delta S}{r_o^2} \quad (2)$$

where $\Delta S = (u_2 - u_1)\,\hat{i} + (v_2 - v_1)\,\hat{j}$. To lowest order

$$u_2 = u_1 + \frac{\partial u}{\partial x}(x_2 - x_1) + \frac{\partial u}{\partial y}(y_2 - y_1)$$

with the corresponding equation for $v_2$. Thus with $(x_2 - x_1)/r_o = \cos\theta$ and $(y_2 - y_1)/r_o = \sin\theta$

$$\epsilon = \cos^2\theta + \frac{\partial v}{\partial y}\sin^2\theta + \left(\frac{\partial u}{\partial y} + \frac{\partial v}{\partial x}\right)\sin\theta\cos\theta \quad (3)$$

We define three quantities $\epsilon_x$, $\epsilon_y$, and $\epsilon_{xy}$ by

$$\epsilon_x = \frac{\partial u}{\partial x}; \quad \epsilon_y = \frac{\partial v}{\partial y}; \quad \epsilon_{xy} = \frac{1}{2}\left(\frac{\partial u}{\partial y} + \frac{\partial v}{\partial x}\right) \quad (4)$$

Notice that $\epsilon_{xy} = \epsilon_{yx}$. With these definitions the elongation becomes

$$\epsilon = \epsilon_x \cos^2\theta + \epsilon_y \sin^2\theta + 2\,\epsilon_{xy} \sin\theta\cos\theta \quad (5)$$

It can be shown that the quantities $\epsilon_x$, $\epsilon_y$, $\epsilon_{xy}$ transform as the components of a tensor, thus these quantities are known as the strain tensor; $\epsilon_x$ and $\epsilon_y$ are normal components and $\epsilon_{xy}$ is the shear component.

In general, survey data does not determine the absolute level of strain since the unstrained distance between points is not known. Rather survey data is used to study the rate of strain accumulation. For many purposes the knowledge of strain rate is as important or more important than the knowledge of the absolute level of strain. If, for example, an earthquake results in a strain decrease, $\Delta\epsilon$, in a certain region, then the next earthquake is likely to occur when the same amount of additional strain reoccurs in the rock body. If the rate at which strain is accumulating is known, a prediction can then be made as to the time of occurrence of the next comparable earthquake. Suppose the rates of strain accumulation are constant between an initial survey time and some later time, $\Delta t$, it follows that

$$\dot{r} = r_o \left[\dot{\epsilon}_x \cos^2\theta + \dot{\epsilon}_y \sin^2\theta + 2\dot{\epsilon}_{xy} \sin\theta\cos\theta\right] \tag{6}$$

The unknowns in this equation are $\dot{\epsilon}_x$, $\dot{\epsilon}_y$, and $\dot{\epsilon}_{xy}$. The quantity known from the resurvey is $\dot{r} = \Delta r/\Delta t$.

For determining the two dimension strain rate tensor a minimum of three lines must be resurveyed; in three dimensions six lines possibly between four sites are required. In the more typical case many more lines are surveyed than required in order to mitigate the effects in measurement noise. The lines are frequently resurveyed a number of times. In this case the observed intersite distances measured for each line at the several different measurement times can be fit to a linear regression line of the form

$$r_i\,(t) = a_i + \dot{r}_i\, t \tag{7}$$

where we have arbitrarily chosen the time of the initial survey at $t = 0$. The elongation rates, $\dot{r}$, determined by the least squares analysis have a variance, $\sigma_{\dot{r}_i}$, which can be deduced by considering the variation in the least squares solution

for $r_i$. We find

$$\sigma^2_{\dot{r}_i} = \frac{n}{n\sum_1^n t_i^2 - \left(\sum_1^n t_i\right)^2}\,\sigma^2_{r_i} \tag{8}$$

where n is the number of measurements of the intersite distances of the $r_i$ line and $\sigma_r^2$ is the variance in $r_i$. If the measurements are made at time intervals $\Delta t$ years apart, then at the end of T years

$$\sigma^2_{\dot{r}_i} = \frac{12(n-1)}{n(n+1)}\,\frac{\sigma^2_{r_i}}{T^2} = \frac{12\frac{T}{\Delta t}}{\left(\frac{T}{\Delta t}+1\right)\left(\frac{T}{\Delta t}+2\right)}\,\frac{\sigma^2_{r_i}}{T^2} \tag{9}$$

Notice that the variances in $\dot{r}_i$ are equal for n = 2 and n = 3, and decrease s'owly for n > 3. As expected the variance in the line rate decreases with increasing duration of the measurement program T.

Once the line rates have been determined they can be used in a regression analysis for the strain rate tensor. We rewrite the system of equations for the elongations as

$$\begin{bmatrix} \dot{r}_1 \\ \dot{r}_2 \\ \cdot \\ \cdot \\ \cdot \\ \dot{r}_n \end{bmatrix} = \begin{bmatrix} r_{o_1}\ell_1^2 & r_{o_1}m_1^2 & r_{o_1}2m_1\ell_1 \\ r_{o_2}\ell_2^2 & r_{o_2}m_2^2 & r_{o_2}2m_2\ell_2 \\ \cdot & & \\ \cdot & & \\ r_{o_n}\ell_n^2 & r_{o_n}m_n^2 & r_{o_n}2m_n\ell_n \end{bmatrix} \begin{bmatrix} \dot{\epsilon}_x \\ \dot{\epsilon}_y \\ \dot{\epsilon}_{xy} \end{bmatrix} \tag{10}$$

or

$$\dot{R} = A\dot{E} \tag{11}$$

where $\ell_i$ and $m_i$ are the direction cosines of the $i^{th}$ line with respect to the x and y axis.

The preceding set of equations can again be solved by least squares techniques to yield

$$\dot{E} = (A^T A)^{-1} A^T \dot{R} \tag{12}$$

where $A^T$ is the transpose of A. (We have written equation 12 in the form appropriate to the case where all the deduced line rates are equally weighted in the solution. When unequal weights are used, the solution is $(A^T w^{-1} A)^{-1} A^T w^{-1} \dot{R}$, where $w^{-1}$ is a weight matrix. Similarly the line rates can also be determined by a weighted least squares analysis of the intersite distances.)

Several properties of the least square solution deserve particular attention. Consider the A matrix; its dimensionality is $n \times 3$. However, in determining $\dot{E}$ it does not appear by itself but in the combinations $A^TA$ and $A^T\dot{R}$. The matrix $(A^TA)$ has dimensions $3 \times 3$; its inverse is called the variance-covariance matrix for reasons discussed below. Straightforward algebraic analysis shows

$$A^T A = \sum_1^n A_i^T A_i$$

$$\begin{bmatrix} \sum_1^n \ell_i^4 r_{o_i}^2 & \sum_1^n \ell_i^2 m_i^2 r_{o_i}^2 & \sum_1^n 2\ell_i^3 m_i r_{o_i}^2 \\ \sum_1^n m_i^2 \ell_i^2 r_{o_i}^2 & \sum_1^n m_i^4 r_{o_i}^2 & \sum_1^n 2m_i^3 \ell_i r_{o_i}^2 \\ \sum_1^n 2m_i \ell_i^3 r_{o_i}^2 & \sum_1^n 2m_i^3 \ell_i r_{o_i}^2 & \sum_1^n (2m_i \ell_i)^2 r_{o_i}^2 \end{bmatrix} \tag{13}$$

where $A_i$ is a $3 \times 1$ row vector corresponding to the $i^{th}$ row of A. Similarly $A^T\dot{R}$ is a three component vector

$$A^T\dot{R} = \begin{bmatrix} \sum_1^n \dot{r}_i \ell_i^2 r_{o_i}^2 \\ \sum_1^n \dot{r}_i m_i^2 r_{o_i}^2 \\ \sum_1^n \dot{r}_i 2m_i \ell_i r_{o_i}^2 \end{bmatrix} \tag{14}$$

Thus, in order to determine the strain rates there is no need to store the potentially large matrix A, only the smaller symmetric matrix $A^TA$ and the $A^T\dot{R}$ vector.

The variance-covariance matrix $(A^TA)^{-1}$ has a very important physical interpretation. When multiplied by the variance in the lines rates, $\sigma_{\dot{r}}^2$, the diagonal elements give the mean squared precision in the deduced elements of the strain rate tensor, while the off diagonal elements give the covariance or overlap between components. Using the diagonal terms

$$\sigma_{\dot{\epsilon}_x}^2 = (A^TA)_{11}^{-1} \sigma_{\dot{r}}^2 \tag{15a}$$

$$\sigma_{\dot{\epsilon}_y}^2 = (A^TA)_{22}^{-1} \sigma_{\dot{r}}^2 \tag{15b}$$

$$\sigma_{\dot{\epsilon}_{xy}}^2 = (A^TA)_{33}^{-1} \sigma_{\dot{r}}^2 \tag{15c}$$

where $\sigma_{\dot{r}}^2$ is given either by equation 8 or 9. Equations 15 are in a very useful form for error analysis. The variance-covariance matrix contains the geometric factors of the solution, namely the lengths of the lines between sites, the number of lines, and their spatial orientations. On the other hand $\sigma_{\dot{r}}^2$ contains the measurement uncertainties in the intersite distances, the frequency of measurement,

and the total time span over which the measurements are made. Scaling relationships can be used to deduce expected precisions for systems with various grid sizes, measurement periods and intersite distance uncertainties from results obtained from the analysis of one system. Thus if the scaling relationships are:

$$r_o' = a\, r_o \tag{16a}$$

$$\Delta t' = b\, \Delta t \tag{16b}$$

$$\Delta r' = c\, \Delta r \tag{16c}$$

then

$$\sigma_{\dot{\epsilon}}' = \frac{c}{ab}\, \sigma_{\dot{\epsilon}} \tag{17}$$

We will consider in the next several paragraphs the estimated errors in deduced strain rates for a variety of cube corner configurations and measurement periods.

One of many possible configurations of targets is shown in Figure 3. The minimum intersite spacing is 25 kilometers, a number chosen from the fact that shorter baselines can be economically and efficiently surveyed by conventional ground techniques. The longest nearest neighbor baselines do not exceed 100 kilometers since it is likely that there are considerable variations in the strain rate over longer distances (and possibly shorter ones). The coordinate system is defined with the positive x axis pointing east and the positive y axis pointing North. We will consider results obtained for five specific subnetworks shown in Figure 4. The number of intersite lines varies from three for the simple triangular configurations to 36 for a nine station square grid. It is a straightforward procedure to use results obtained with these subnetworks to obtain results using the same subnetworks in different orientations relative to the coordinate axes. If $\theta$ is the angular distance by which a new coordinate system is rotated from the old system then

$$\begin{bmatrix} \dot{\epsilon}'_x \\ \dot{\epsilon}'_y \\ \dot{\epsilon}'_{xy} \end{bmatrix} = \begin{bmatrix} \cos^2\theta & \sin^2\theta & 2\cos\theta\sin\theta \\ \sin^2\theta & \cos^2\theta & -2\sin\theta\cos\theta \\ -\sin\theta\cos\theta & \sin\theta\cos\theta & \cos^2\theta - \sin^2\theta \end{bmatrix} \begin{bmatrix} \dot{\epsilon}_x \\ \dot{\epsilon}_y \\ \dot{\epsilon}_{xy} \end{bmatrix} \quad (18)$$

where the primed values are the strain rates relative to the new coordinate axes. We also should note that the strain rate tensor can be diagonalized, that is, there is a coordinate system in which the shear strain vanishes and the strain is represented in this coordinate system by the values of the normal components called the principle strain rates.

Figures 5-9 show the standard deviations in the deduced strain rates, $\dot{\epsilon}_x$, $\dot{\epsilon}_y$, $\dot{\epsilon}_{xy}$, for the subnetworks of Figure 4 as a function of the total period of the measurement program, T, and the time between each resurvey, $\Delta t$. The results are normalized to a 1 cm noise in the baseline determinations and can be scaled to other values of noise accordingly. The simple triangular configuration of Figure 4a gives equally precise determinations of all three components of the strain rate (Figure 5). The precision improves from about $5 \times 10^{-7}$ $yr^{-1}$ after one year to about $1.5 - 3.5 \times 10^{-7}$ $yr^{-1}$ after 15 years. These numbers should be compared with the expected strain rates for a system such as the strike-slip San Andreas Fault System in California. Orienting the coordinate axes so that the fault trace is aligned roughly with the y axis, measurements near the fault suggest shear strain rates of about $7 \times 10^{-7}$ $yr^{-1}$ and normal strain rates somewhat less. (Scholz and Fitch, 1969). It is clear then that the simple triangular subnetwork of sites spaced 25 kilometers apart is barely adequate for measuring the expected strain rates in the time frame of one or two decades. The situation improves considerably as we consider other subnetworks with more reflector sites and longer

baselines (Figures 6-9). Figure 7 shows that with a square configuration of sites and six baselines the precision in both the normal and shear components of straining is about 1.5 - 3.5 $\times 10^{-8}$ $yr^{-1}$ after ten years. Even better, with the nine site configuration of Figure 5e, we obtain in two years a precision of 4-5 $\times 10^{-8}$ $yr^{-1}$ in the normal component and 3-4 $\times 10^{-8}$ $yr^{-1}$ in the shear component, as shown in Figure 9. Using the expected shear strain rate of 7 $\times 10^{-7}$ $yr^{-1}$ and assuming a baseline noise of one centimeter our analysis suggests a signal-to-noise ratio of 20:1. After fifteen years the signal-to-noise ratio improves to about 280:1. Even using more conservative figures for the noise in the baseline determinations, say two or three centimeters, yields very satisfactory signal-to-noise ratios. We conclude that relatively simple configurations of sites can be used suitably spaced for very precise determinations of strain rates in a relatively short periods of time. In locations where various factors do not permit the density of sites to be as high as used in this analysis, simple configurations using longer baselines of say 100 kilometers, and longer measurement periods, T, may be used instead. With such a subnetwork more attention has to be given to consideration of the uniformity of the strain rate over the extended spatial width and temporal span employed. Thatcher (1977) has obtained results suggesting that, at least in some places in California, uniform straining extends over a deformation zone of 100 kilometers or more. One major use of a SGRS system can be to determine more fully the spatial extent of the straining and the rate at which the straining decreases as one moves away from major faults at, say, tectonic plate boundaries.

The results we have presented in Figures 5-9 suggest a relatively weak dependence of the strain rate precision on the frequency of resurveying. While this is true in principle, it is somewhat misleading in practice. The analysis assumes

an a-priori knowledge of the precision in the baseline determinations. In general such knowledge is obtained only by surveying frequently enough to obtain statistically reliable data for analysis of the baseline precisions.

We should also take note of the possibility of detecting time dependent changes in the strain rates should they occur. If such changes are a significant fraction of the strain rate, then the simulation results in, say, Figure 9 suggest such changes might be detected with time scales of a decade or two.

## IV. SUMMARY

We have performed an analysis of the precision with which strain rates can be derived from a determination of baseline between various locations. We have applied this analysis to surveys which might be made with a Spaceborne Geodynamics Ranging System using the precisions expected for this system. The results indicate that with realistic subnetwork configurations of target sites, the strain rate tensor can be deduced to precisions of a few parts in $10^8$ in periods of several years. Precisions better than one part in $10^8$ may be possible with programs spanning a few decades or with sophisticated measurement and analysis techniques. Among the potential applications for SGRS are:

1. the determination of the rates of crustal strain simultaneously at many diverse locations,
2. the study of spatial variations in straining in broad deformation zones,
3. the study of temporal variations in strain rates over the time span of, say, a decade should such variations exist.

Other applications may also become apparent as our knowledge of the system capabilities improves and our techniques of data processing become more sophisticated.

Acknowledgments

The authors thank Werner Kahn for many enlightening conversations on least squares analysis and SGRS concepts. They also express their appreciation to Michael Fitzmaurice for discussing the engineering status of the system. The form for $\sigma_{\dot{r}}^2$ used in equation 9 was brought to our attention by Michael Chinnery.

## References

Gibbs, B. P., and E. M. Haley, "Error Analysis of the Spacelab Geodynamics Laser Ranging System," Final Report NASA Contract NAS 5-23715, 1978.

Scholz, C. H., and T. J. Fitch, "Strain Accumulation along the San Andreas Fault," J. Geophys. Res., 27, 6649-6666, 1969.

Thatcher, W., "Secular Deformation and the Earthquake Cycle on the San Andreas Fault," EOS, Trans. Am. Geophys U., 58, 1227, 1977.

Vonbun, F. O., W. O. Kahn, P. O. Argentiero, and D. W. Koch, "Spaceborne Earth Applications Ranging System (SPEAR)," Journal of Spacecraft and Rockets, 14, 492-495, 1977.

Table I

| | |
|---|---|
| **Transmitter pulse energy** | 50 millijoules |
| **Transmitter wavelength** | 0.53 $\mu$meters |
| **Pulse frequency** | 0.1 seconds |
| **Transmitter divergence** | 0.5 milliradians |
| **Lidar cross section of reflective area** | $5 \times 10^6$ square meters 20° elevation |
| | $1 \times 10^6$ square meters 90° elevation |
| **Receiver area** | $7.3 \times 10$ square meters |
| **Signal-to-noise ratio** | 7 db at 20° elevation |
| | 20 db at 90° elevation |

Engineering specifications for SGRS prototype under development for proposed use on Space Shuttle.

## FIGURE CAPTIONS

**Figure 1.** Conceptual representation of SGRS measurement. The vector $r_{12}$ is the intersite vector between two target sites.

**Figure 2.** Analysis of strain in two dimensions. The line has length $r_o$ in unstrained state and length r in strained state.

**Figure 3.** A possible configuration of SGRS reflective targets sites. A total of 56 sites are spread over a grid 375 km. long and 150 km. wide. A hypothetical fault cutting through the grid is shown as a continuous line.

**Figure 4.** Representative subnetworks of Figure 3. For n sites in a subnetwork, the potential number of lines is $n(n-1)/2$ (e.g. 36 lines in e).

**Figure 5.** Precision in the deduced values of the strain rates, $\dot{\epsilon}_x$, $\dot{\epsilon}_y$, $\dot{\epsilon}_{xy}$, for the subnetwork shown in Figure 4a as a function of the total duration of the measurement program, T and the resurvey period $\Delta t$.

**Figure 6.** Precision in the deduced values of the strain rates, $\dot{\epsilon}_x$, $\dot{\epsilon}_y$, $\dot{\epsilon}_{xy}$, for the subnetwork shown in Figure 4b as a function of the total duration of the measurement program, T and the resurvey period $\Delta t$.

**Figure 7.** Precision in the deduced values of the strain rates, $\dot{\epsilon}_x$, $\dot{\epsilon}_y$, $\dot{\epsilon}_{xy}$, for the subnetwork shown in Figure 4c as a function of the total duration of the measurement program, T and the resurvey period $\Delta t$.

**Figure 8.** Precision in the deduced values of the strain rates, $\dot{\epsilon}_x$, $\dot{\epsilon}_y$, $\dot{\epsilon}_{xy}$, for the subnetwork shown in Figure 4d as a function of the total duration of the measurement program, T and the resurvey period $\Delta t$.

Figure 9. Precision in the deduced values of the strain rates, $\dot{\epsilon}_x$, $\dot{\epsilon}_y$, $\dot{\epsilon}_{xy}$ for the subnetwork shown in Figure 4e as a function of the total duration of the measurement program, T and the resurvey period $\Delta t$.

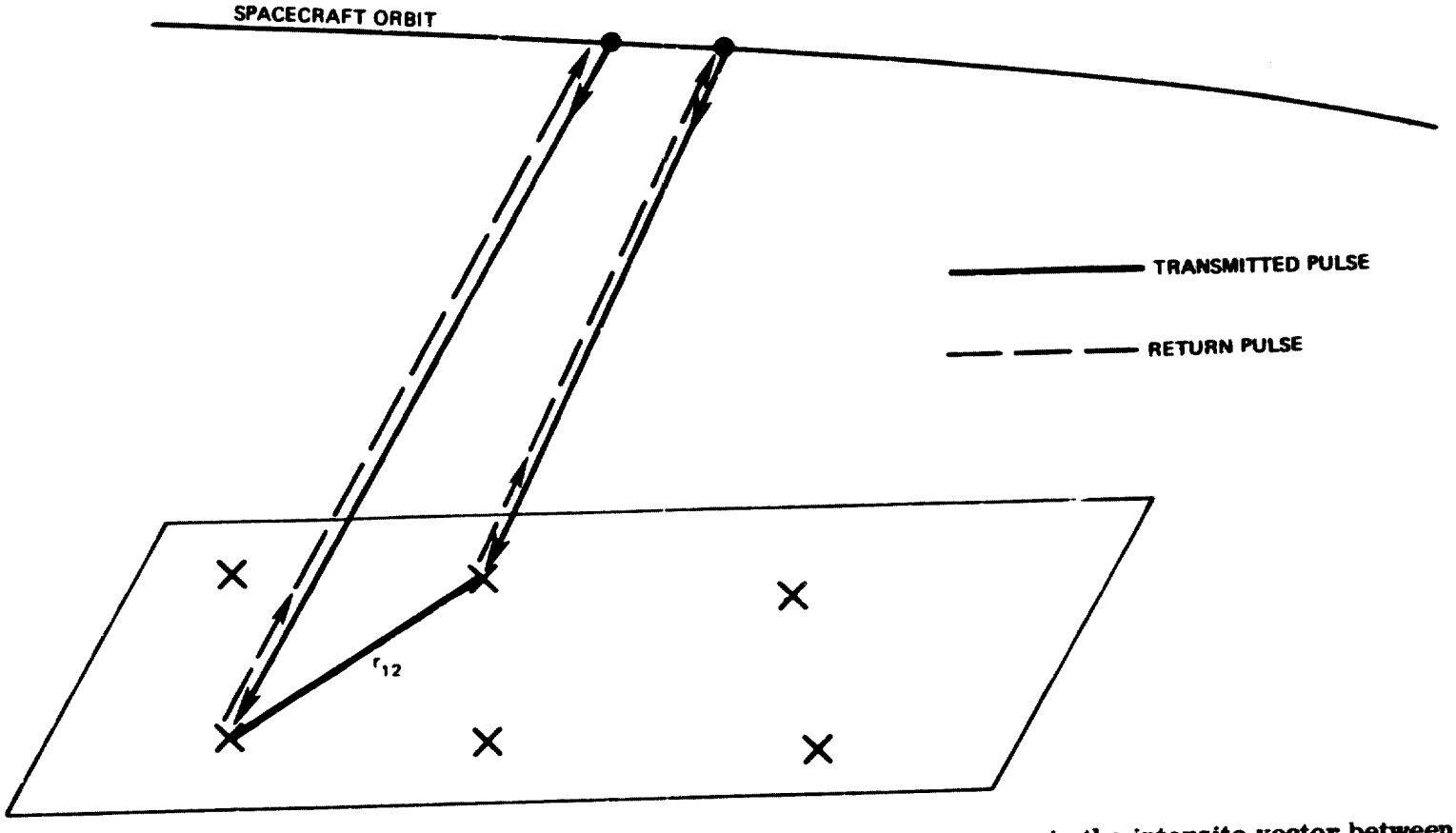


Figure 1. Conceptual representation of SGRS measurement. The vector $r_{12}$ is the intersite vector between two target sites.

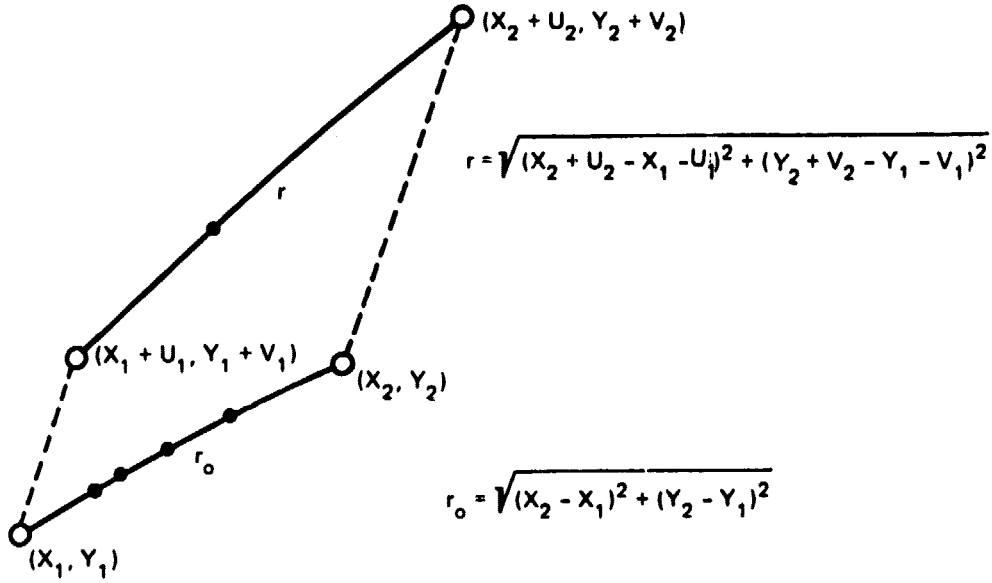


**Figure 2. Analysis of strain in two dimensions. The line has length $r_o$ in unstrained state and length r in strained state.**

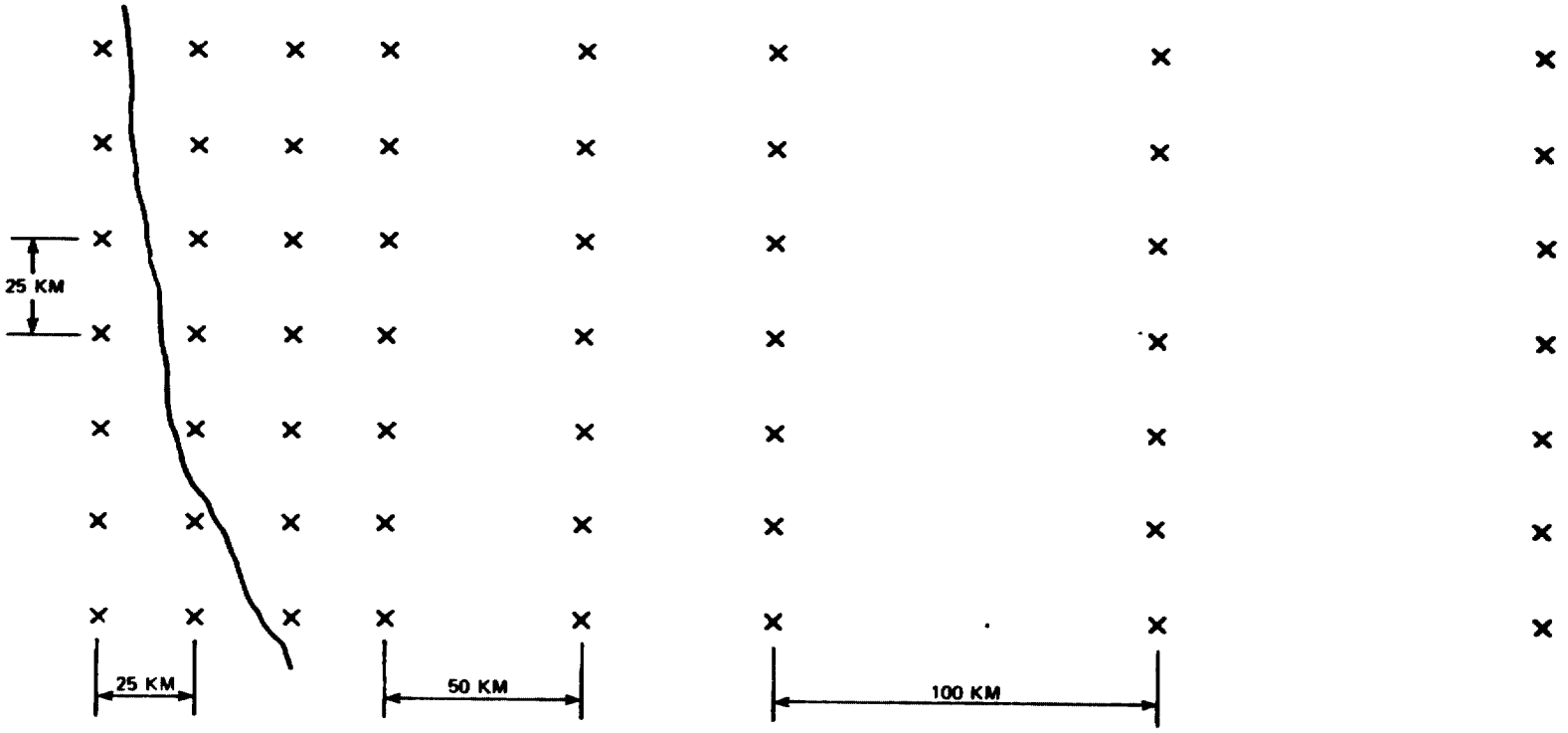


Figure 3. A possible configuration of SGRS reflective targets sites. A total of 56 sites are spread over a grid 375 km. long and 150 km. wide. A hypothetical fault cutting through the grid is shown as a continuous line.

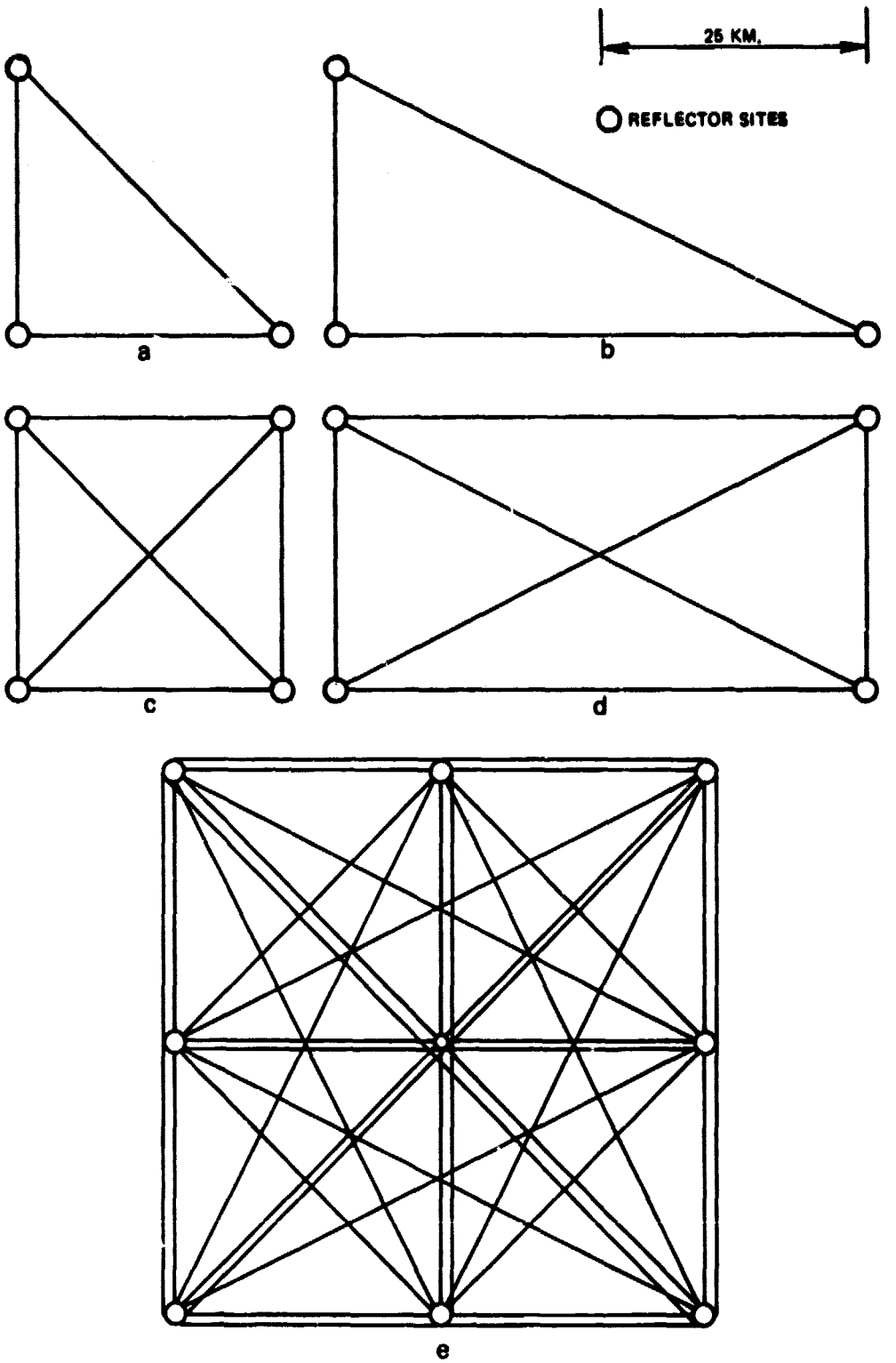


Figure 4. Representative subnetworks of Figure 3. For n sites in a subnetwork, the potential number of lines is $n(n-1)/2$ (e.g. 36 lines in e).

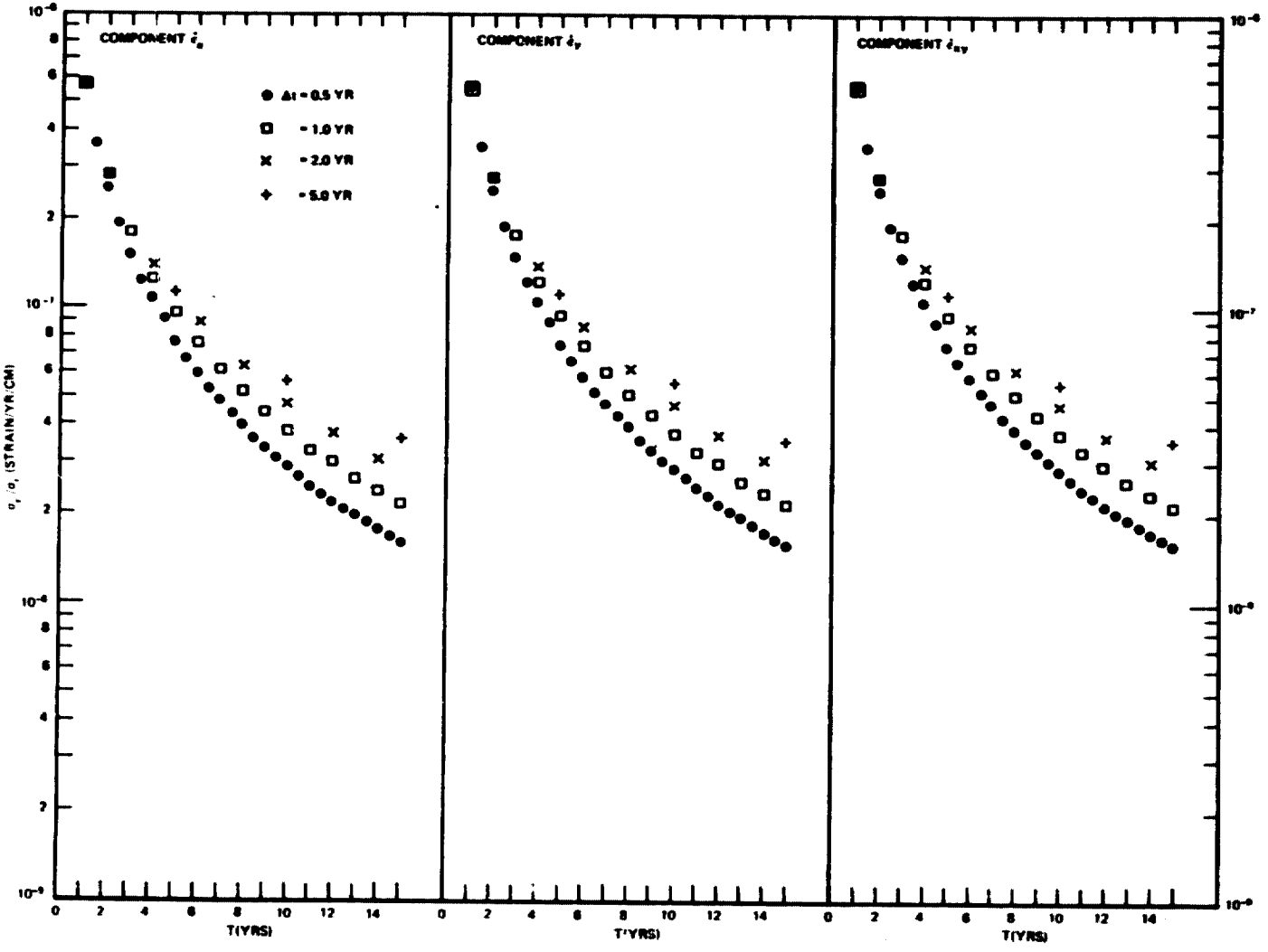


**Figure 5.** Precision in the deduced values of the strain rates, $\dot{\epsilon}_x$, $\dot{\epsilon}_y$, $\dot{\epsilon}_{xy}$, for the subnetwork shown in Figure 4a as a function of the total duration of the measurement program, T and the resurvey period $\Delta t$.

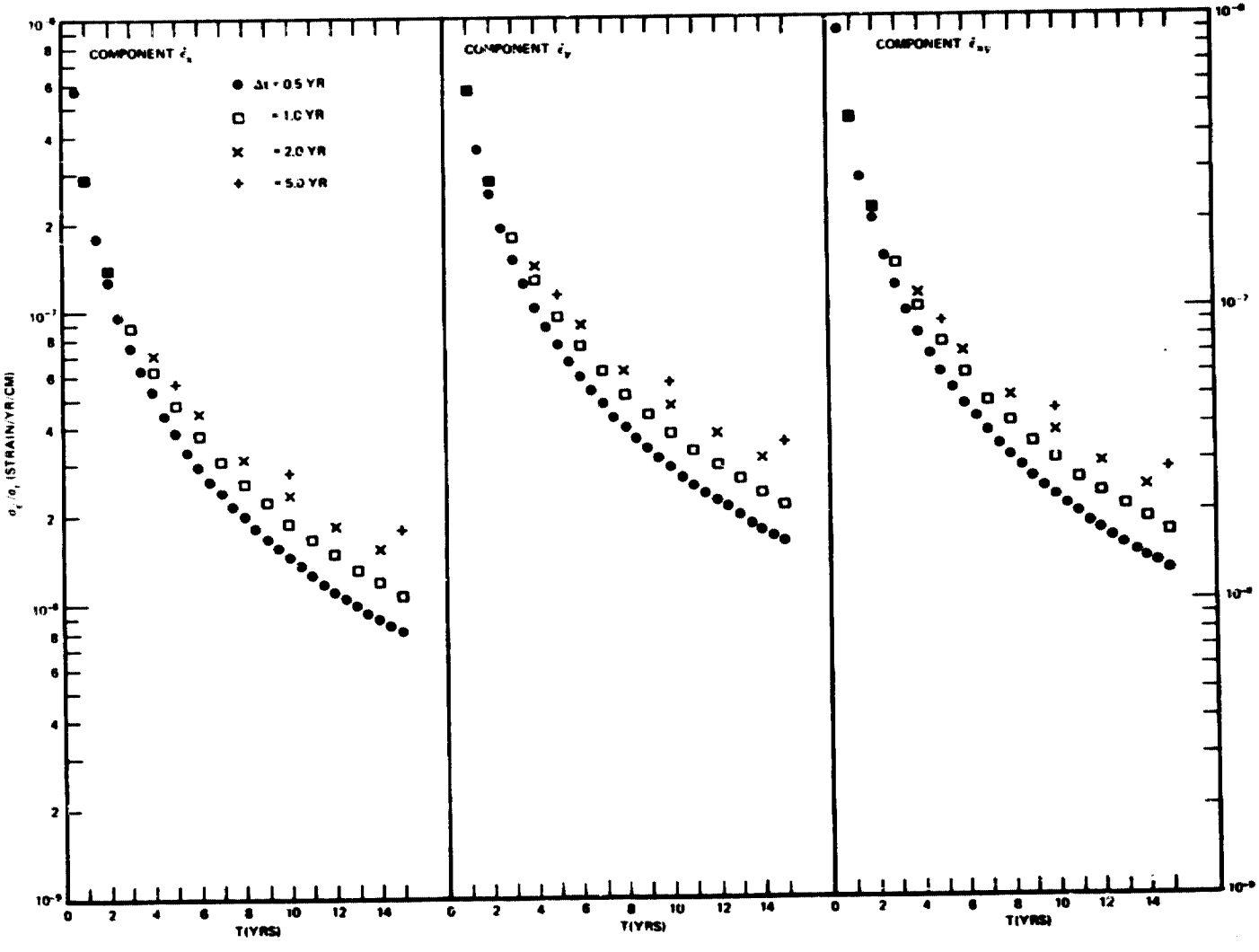


**Figure 6. Precision in the deduced values of the strain rates, $\dot{\epsilon}_x$, $\dot{\epsilon}_y$, $\dot{\epsilon}_{xy}$, for the subnetwork shown in Figure 4b as a function of the total duration of the measurement program, T and the resurvey period Δt.**

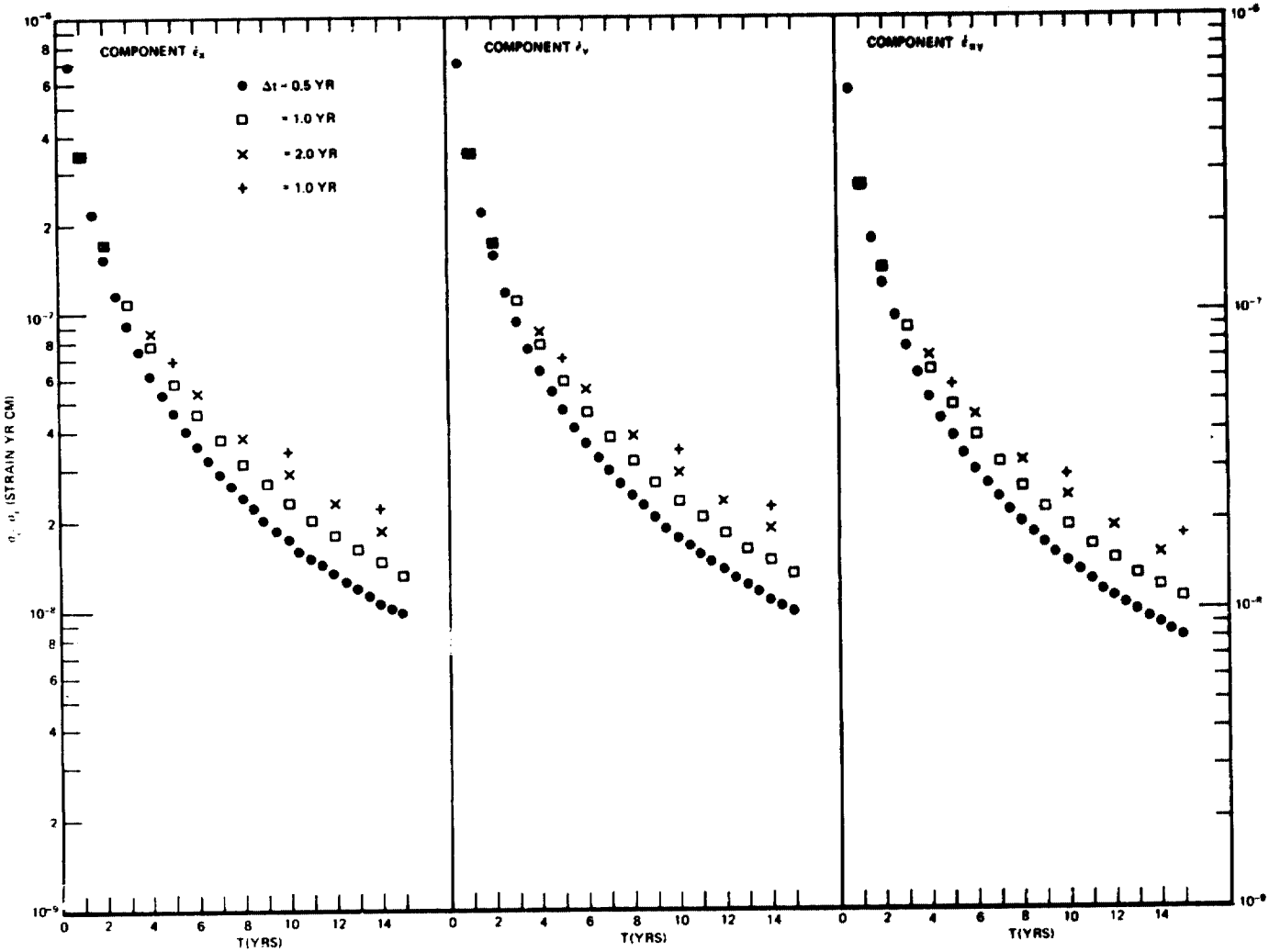


Figure 7. Precision in the deduced values of the strain rates, $\dot{\epsilon}_x$, $\dot{\epsilon}_y$, $\dot{\epsilon}_{xy}$, for the subnetwork shown in Figure 4c as a function of the total duration of the measurement program, T and the resurvey period $\Delta t$.

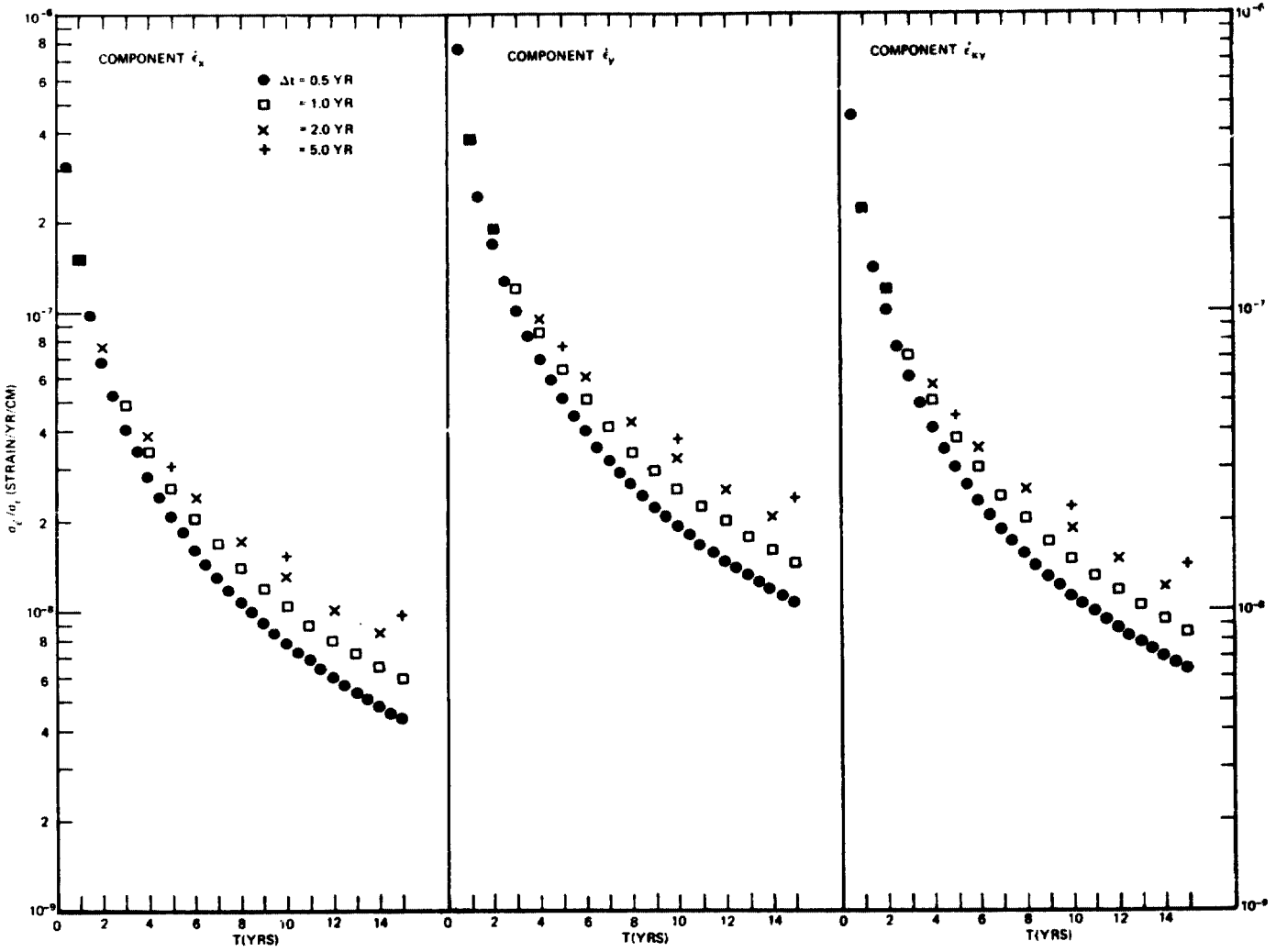


Figure 8. Precision in the deduced values of the strain rates, $\dot{\epsilon}_x$, $\dot{\epsilon}_y$, $\dot{\epsilon}_{xy}$, for the subnetwork shown in Figure 4d as a function of the total duration of the measurement program, T and the resurvey period $\Delta t$.

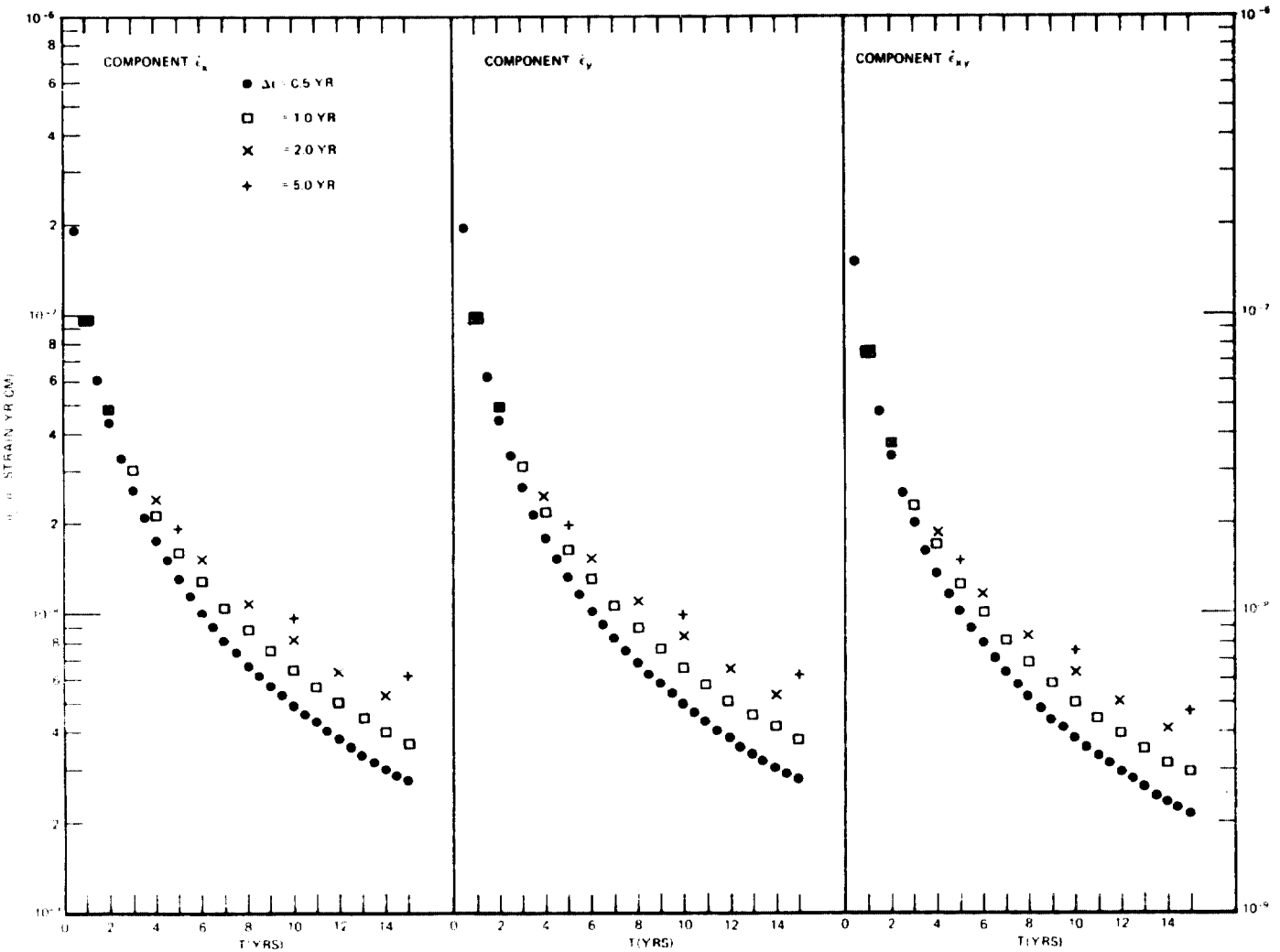


Figure 9. Precision in the deduced values of the strain rates, $\dot{\epsilon}_x$ , $\dot{\epsilon}_y$, $\dot{\epsilon}_{xy}$, for the subnetwork shown in Figure 4e as a function of the total duration of the measurement program, T and the resurvey period $\Delta t$.